Ceramics International 42 (2016) 16969–16980

Contents lists available at ScienceDirect

Ceramics International

journal homepage: www.elsevier.com/locate/ceramint

Introduction of novel kinetic approach to calculation of activation energy and its application to the sinter-crystallization of strontian feldspar

Petr Ptáček *, Tomáš Opravil, František Šoukal

Brno University of Technology, Faculty of Chemistry, Centre for Materials Research CZ.1.05/2.1.00/01.0012, Purkyňova 464/118, Brno CZ-612 00, Czech Republic

ARTICLE INFO

Article history:
Received 30 June 2016
Received in revised form
21 July 2016
Accepted 28 July 2016
Available online 29 July 2016

Keywords:
Strontian feldspar
Sr-celsian
Ceramics
Kinetics
Thermodynamics
Activated complex

ABSTRACT

The kinetics, the mechanism and the thermodynamics of activated state of formation of primary strontian feldspar via sinter-crystallization of non-equilibrium melt during the thermal treatment of ceramic body was investigated in this work via differential thermal analysis using isoconversional Kissinger kinetic equation. The process of formation of non-equilibrium melt and subsequent crystallization of primary strontian feldspar requires the activation energy of 631 ± 3 and 664 ± 2 kJ mol^{-1}, respectively. The investigation of mechanism of formation of primary strontian feldspar reveals that the process is driven by the surface nucleation and diffusion controlled growth of the new phase. The nucleation rate decreases with the time of process and non-equilibrium melt can be formed only in metastable equilibrium with activated state of strontian feldspar. Deep consideration of kinetic data leads to the deduction of new kinetic approach that enables single calculation of activation energy and frequency factor of heterogeneous processes as well as the dependence of thermodynamic parameters of activated state on temperature. Further consideration of kinetic data reveals that the activation energy is directly proportional to the function of *csch* $(\boldsymbol{z})+1$. For $\boldsymbol{z}=\boldsymbol{e}$, this term enables to derive the value for the parameter $\boldsymbol{B}(\boldsymbol{x})$ in empirical equation for Arrhenius temperature integral $\boldsymbol{p}(\boldsymbol{x})$ proposed by Doyle to be 1.0642.

1. Introduction

Feldspars are intensively studied due to their importance in petrography [1,2], understanding the Earth's geology [2,3], soil sciences, where some clay minerals are produced by weathering of feldspars directly or through intermediate phases [4,5], as well as in the production of ceramics, glass and glass-ceramics [6–9]. Ground rocks of potassium feldspar have also wide efficiency as a fertilizer [10]. The composition of this subclass of silicate minerals, i.e. tectosilicates with Al-Si framework [11], is described by the formula MT_4O_8 (or $M_xT_yO_8$, where $\boldsymbol{y}$ reaches 4 and the parameter $\boldsymbol{x}$ does not fall below 0.975 [12]). Feldspars are the most abundant minerals in the Earth's crust (60–64% by weight) [13,14]. **T**-sites (aluminosilicate framework) are occupied by small strongly charged cations (typically Si^{4+} and Al^{3+}) and **M**-sites (interstices) are occupied by larger, weakly charged cations (Na^+, K^+, Ca^{2+}, Sr^{2+}, Ba^{2+}, …). Feldspars can be characterized by the content of all 92 naturally occurring elements [12]. In Na- and K-feldspars, Si^{4+} and Al^{3+} can be completely replaced by Ga^{3+} and Ge^{3+} [15].

Synthetic strontian feldspar (Sr-celsian, strontium aluminosilicate feldspar, SAS, $SrAl_2Si_2O_8$) is of great technological interest due to low thermal expansion coefficient [16,17]), low and thermally stable dielectric constant, low dielectric losses, high mechanical strength, chemical inertness, and high melting temperature. Therefore they are known as the materials for the matrix of fiber-reinforced ceramic composites, protective coatings, electro-ceramics and refractories [18–25] as well as for the preparation of glass ceramics [26–28] and luminescent pigments of $MAl_2Si_2O_8:X^{n+}$; where M = Ca, Sr, Ba and X^{n+} denotes ions of doped element [29–35].

Previous investigation of reaction mechanism, kinetics and thermodynamics of the process of formation of synthetic strontian feldspar via ceramic route [36] revealed that the main reaction pathway is initiated by the thermal decomposition of $SrCO_3$ and continues with the formation of binary oxide intermediates and primary strontian feldspar via the crystallization from non-equilibrium melt. The reactions between intermediates or the reaction of these intermediates with SiO_2 and Al_2O_3 leads to the formation of secondary strontian feldspar. Large plate-like particles of

* Corresponding author.
E-mail addresses: ptacek@fch.vutbr.cz (P. Ptáček), opravil@fch.vutbr.cz (T. Opravil), soukal@fch.vutbr.cz (F. Šoukal).

http://dx.doi.org/10.1016/j.ceramint.2016.07.203

tertiary strontian were formed by recrystallization of primary and secondary strontian feldspar. The formation of strontian within the temperatures over 1150 °C is driven by the kinetics of chemical reaction of 1.5 order and requires the average apparent activation energy of 229.3 kJ mol^{-1}.

This work expands these foundations by detailed investigation of reaction mechanism, kinetics and thermodynamic of the process of formation of synthetic primary strontian feldspar as an essential part of the main reaction pathway. The investigation of kinetic results and thermodynamic data of activated state enables to formulate proper equations to determine the activation energy, the frequency factor as well as the relations describing the dependence of enthalpy, entropy, volume and density of transition state on temperature. Since the synthetic strontian feldspar was sometimes abbreviated as strontian in the text of previous work [36], in order to avoid confusion with the mineral strontianite [37], this abbreviation is not used in this work.

2. Experimental

2.1. Synthesis and analysis of properties of sample

Raw meal for the synthesis of strontian feldspar was prepared by mixing strontium carbonate ($SrCO_3$), alumina (Al_2O_3) and silica (SiO_2) in the mass ratio of 1.45:1:1.18, which corresponds to the stoichiometric composition of $SrAl_2Si_2O_8$ ($SrO \cdot Al_2O_3 \cdot 2SiO_2$). The initial homogenization of raw meal was performed by short milling (5 min) with vibration laboratory mill. The kinetics of formation of primary strontian feldspar during the thermal treatment of raw meal was investigated by TG-DTA (TG-DTA analyzer SDT Q600). 30 mg of sample were heated in the air conditions (100 cm^3 min^{-1}) under the rate from 5 to 20 °C min^{-1}. The other aspects of the process of strontian feldspar synthesis are described in previous work [36].

2.2. Applied kinetic approach

The kinetic triplet of the process includes the information about the activation energy, the frequency factor and the mechanism. The apparent activation energy ($\boldsymbol{E}_a$) and the frequency factor ($\boldsymbol{A}$) of investigated process were evaluated by the mechanism-free maximum rate (peak) method of type B [38] based on the Kissinger kinetic approach [39–41]. The peak temperature ($\boldsymbol{T}_m$), i.e. the temperature at which the rate of investigated process ($d\boldsymbol{\alpha}/d\boldsymbol{t}$) reaches its maximum, is a stationary point where the transformation rate is equal to zero [38,40,42,43]:

$$\frac{d\,\alpha}{d\,t} = f(\alpha)\,k(T) = 0 \tag{1}$$

where α is the fractional conversion, $\boldsymbol{t}$ is the time and $\boldsymbol{k}(\boldsymbol{T})$ is the proportionality factor known as the rate constant at absolute temperature $\boldsymbol{T}$. α (fraction reacted [44]) is readily determined as a fractional change of any physical property associated with the reaction progress, e.g. the mass change during the thermal decomposition of solids [45]:

$$\alpha = \frac{m_0 - m_t}{m_0 - m_f} = \frac{\Delta m}{m_{total}} \tag{2}$$

where $\boldsymbol{m}_0$, $\boldsymbol{m}_t$ and $\boldsymbol{m}_f$ are initial ($\boldsymbol{t}=0$), measured at time $\boldsymbol{t}$ and final masses.

The particular function $f(\alpha)$ which is proportional to the amount of reactant is known as the "kinetic model" (the concept given by Eq. (1) was introduced by Guldberg and Waage[46–48] as the "law of mass action"). Therefore, the temperature dependence of the reaction rate constant is given by the Arrhenius law [49]:

$$k(T) = A\,\exp\left[-E_a/RT\right] \tag{3}$$

it can be further derived [41]:

$$\frac{d^2\alpha}{dt^2} = \frac{d\alpha\left[d\alpha/dt\right]}{dt} = \left(\frac{d\,f(\alpha)}{dt}A\ \exp\left[-\frac{E_a}{RT}\right] + A\ f(\alpha)\frac{d\left[\exp(-E_a/RT)\right]}{dt}\right)_{T=T_m} = 0 \tag{4}$$

Assuming that the heating rate is constant but not equal to zero ($\Theta = d\boldsymbol{T}/d\boldsymbol{t} \neq 0$) and the term $d[exp(-\boldsymbol{E}_a/\boldsymbol{RT})]/d\boldsymbol{t} = \boldsymbol{E}_a\Theta/\boldsymbol{RT}^2 \exp(-\boldsymbol{E}_a/\boldsymbol{RT})$:

$$\frac{d\left[f(\alpha)\right]}{dt} + f(\alpha)\frac{E_a\Theta}{RT^2} = 0 \tag{5}$$

Given the identity $f'(\alpha) = d[f(\alpha)]/d\alpha$ then $d[f(\alpha)]/d\boldsymbol{t} = f'(\alpha)d\alpha/d\boldsymbol{t}$ leads to the equation:

$$A\ \exp\left[-\frac{E_a}{RT_m}\right] f'(\alpha_m)\ + \frac{E_a\Theta}{RT_m^2} = 0 \tag{6}$$

where $\alpha_{\boldsymbol{m}}$ is the fractional conversion (or the degree of transformation [41]) reached for the temperature $\boldsymbol{T}_m$ and $\boldsymbol{R}$ is the universal gas constant (8.314 J K^{-1} mol^{-1}). The term $f'(\alpha_m) \equiv df(\alpha)/d\alpha|_{\alpha=\alpha m}$ is assumed as a constant, i.e. is independent of $\boldsymbol{\Theta}$ or $\boldsymbol{T}_m$. Eq. (6) can be solved for $\Theta/\boldsymbol{T}_m^2$ and expressed via its logarithm form:

$$\ln\left[\frac{\Theta}{T_m^2}\right] = -\frac{E_a}{RT_m} + \ln\left(-\frac{AR}{E_a}f(\alpha_m)\right) \tag{7}$$

For the reaction of first-order ($\boldsymbol{n}=1$), where ($f(\alpha)=1-\alpha$) is $f'(\alpha_m) = -1$ and term $ln(-f'(\alpha)) = 0$, can then be written [41]:

$$\ln\left[\frac{\Theta}{T_m^2}\right] = -\frac{E_a}{RT_m} + \ln\left(\frac{AR}{E_a}\right) \tag{8}$$

A generalized solution of Kissinger equation containing the solution of $f'(\alpha)$ for common forms of $f(\alpha)$, i.e. the reaction mechanism or the kinetic model, and for near equilibrium solid–gas heterogeneous transformations, can be found in works [50–52], respectively.

The combination of the second derivative equation (Eq. (4)) with the kinetic model of Freeman and Carroll [53], where $f(\alpha) = (1-\alpha)^{\boldsymbol{n}}$, leads to the equation for the reaction of nth-type, which can be written as follows [54,55]:

$$\ln\left[\frac{\Theta}{T_m^2}\right] = \ln\left[\frac{AR}{E_a}n(1-\alpha_m)^{n-1}\right] - \frac{E_a}{RT_m} = const. - \frac{E_a}{RT_m} \tag{9}$$

where term $(1-\alpha_m)$ is the fraction of remaining sample, i.e. not reacted [44], which is the constant for given value of $\boldsymbol{n}$. The points on the plot of $ln(\boldsymbol{AR}/\boldsymbol{E}_a)$ versus $\boldsymbol{T}_m^{-1}$ were fitted by the straight line with the slope equal to $-\boldsymbol{E}_a/\boldsymbol{R}$, i.e. $\boldsymbol{E}_a = -\boldsymbol{R}\ (\partial(ln\,\Theta/\boldsymbol{T}_m^2)/\partial(1/\boldsymbol{T}_m))$, whereas the intercept yields to the constant term of Eq. (9). For most kinetic models, the percent error in the calculation of the activation energy is below 2% if $\boldsymbol{E}_a/\boldsymbol{RT}_m > 10$ [41,54,56].

The mechanism was estimated from the shape of DTG peak via the value of kinetic exponent ($\boldsymbol{n}$) which is related to the empirical order of reaction [39]. The exponent can be calculated from the equation derived by Augis and Bennet [57,58]:

$$n = \frac{2.5\,R\,T_m^2}{w_{1/2}\,E_a} \tag{10}$$

where $\boldsymbol{w}_{1/2}$ is a half-width (width at a half height) of peak. The value of kinetic exponent is typical for various mechanisms of the

investigated process [59]. According to this relation, sharp peak (small $w_{1/2}$ and large n) implies a bulk crystallization, while broad peak (small $w_{1/2}$ and large n) signifies a surface crystallization [60]. The value of parameter n can be also determined from the shape index of the DTA peak [51].

2.3. Investigation of thermodynamics of activated state

The calculation of the transition-state thermodynamic functions of investigated process is based on the **Eyring** (or **Eyring-Polanyi**) equation [61], which resembles the **Arrhenius law** (Eq. (3)) [49] for the temperature dependence of the rate constant ($k(T)$) [62–64]:

$$k(T) = \frac{k_B T}{h}\exp\left[\frac{\Delta S^{\#}}{R}\right]\exp\left[-\frac{\Delta H^{\#}}{RT}\right] = \nu \exp\left[-\frac{\Delta G^{\#}}{RT}\right] = \nu K^{\#} \quad (11)$$

where the pre-exponential factor is expressed by the term:

$$A = \kappa\frac{k_B T}{h} \exp\left[\frac{\Delta S^{\#}}{R}\right]\frac{Q^{\#*}}{Q_r} \quad (12)$$

The transitional term, i.e. the ratio of partition functions for rotation and vibration $Q^{\#*}/Q_r$, is usually chosen similar for the reactant (r) and activated complex and can be excluded [65]. The symbols k_B, h and $\nu = k_B T/h$ are the Boltzmann ($1.381 \cdot 10^{-23}$ J K^{-1}), the Plank constant ($6.626 \cdot 10^{-34}$ J s) and the universal vibration frequency, respectively. The value of transmission coefficients κ is in many cases equal to unity [66]. The thermodynamic parameters of activated complex, including the Gibbs free energy ($\Delta G^{\#}$), enthalpy ($\Delta H^{\#}$) and entropy ($\Delta S^{\#}$) of activation process (initial state↔transition state [64]) were calculated using the relations [62,63]:

$$\Delta H^{\#} = E_a - RT; \quad (13)$$

$$\Delta S^{\#} = R\left[\ln\left(\frac{h\ A}{k_B T}\right)\right] \quad [\kappa = 1] \quad (14)$$

and

$$\Delta G^{\#} = \Delta H^{\#} - T\Delta S^{\#}. \quad (15)$$

3. Results and discussion

The kinetics, mechanism and thermodynamics of activated state of the process of sinter-crystallization of primary strontian feldspar from non-equilibrium melt was evaluated from the results of differential thermal analysis. The TG-DTA plot in Fig. 1 (a) shows the behavior of raw meal treated with the heating rate of 5, 7, 10, 15, 17 and 20 °C min^{-1}. The course of synthesis, the reaction between individual components of raw meal and formed intermediates are described in detail in previous work [36]. The change of the peak temperature and other peak parameters (Fig. 1 (b)) during the processes of endothermic formation of non-equilibrium melt (T_{m1} in detail in Fig. 1(a)) and exothermic sinter-crystallization of strontian feldspar (T_{m2}) with the heating rate was utilized for the determination of the kinetic constants of sinter-crystallization process of primary $SrAl_2Si_2O_8$.

The ascertained dependence of peak temperature (T_{mi}, where $i=1$ for the formation of non-equilibrium melt and 2 for the crystallization of primary strontian feldspar) on heating rate (Fig. 2 (a) and (b)) can be accurately fitted by the power law:

$$T_{mi} = a_i\,\Theta^{b_i} = T_{mi,\Theta=1}\Theta^{RT_{mi,\Theta=1}/E_{ai}} \quad (16)$$

where parameter a_i is the peak temperature T_{mi} [K] determined for $\Theta = 1$ K min^{-1} and scaling exponent b_i is given by the dimensionless ratio $RT_{mi,\Theta=1}/E_{ai} = T_{mi,\Theta=1}/T'$, where $T' = E_a/R$ (please refer to Eq. (23)). That means that the peak temperature is proportional to the heating rate raised to the $RT_{mi,\Theta=1}/E_{ai}$ power. The values of these invariables a_1 and b_1 determined for the process of formation of non-equilibrium melt ($R^2 = 0.999$) are 1369.39 ± 1.09 K and $(1.80 \pm 0.03) \cdot 10^{-2}$, respectively. For subsequent process of sinter-crystallization of primary strontian feldspar the values $a_2 = 1405.77 \pm 0.53$ K and $b_2 = (1.784 \pm 0.015) \cdot 10^{-2}$ were assessed ($R^2 = 0.999$). The convenient confidence level of these experimental dependences enables to fit and broaden investigated interval of heating rate to the range from 1 to 30 °C min^{-1} (Fig. 2).

The apparent activation energy and the constant term for the computation of frequency factor were determined from the slope of logarithmic form of Kissinger equation (Eq. (9)), which was depicted in Fig. 3 in usual form of Kissinger plot. The overview of kinetic results derived from experimental and the sum of experimental and extrapolated data are listed in Table 1.

The value of E_{a1}, i.e. the apparent activation energy of the process of formation of non-equilibrium melt, is determined to be 633 ± 24 kJ mol^{-1} (a). The value of E_{a1} calculated from the sum of experimental and calculated peak temperatures is 631 ± 3 kJ mol^{-1} (please refer to the detail of Fig. 3(a)). The process of sinter-crystallization of primary strontian feldspar requires the activation energy (E_{a2}) of about 658 ± 7 kJ mol^{-1} (b). The apparent activation energy resulting from the combination of both sets of data, i.e. the experimental and the calculated points, is 664 ± 2 kJ mol^{-1} (detail of Fig. 3 (b)). The original and extended sets of data are in satisfying conformity for both investigated processes.

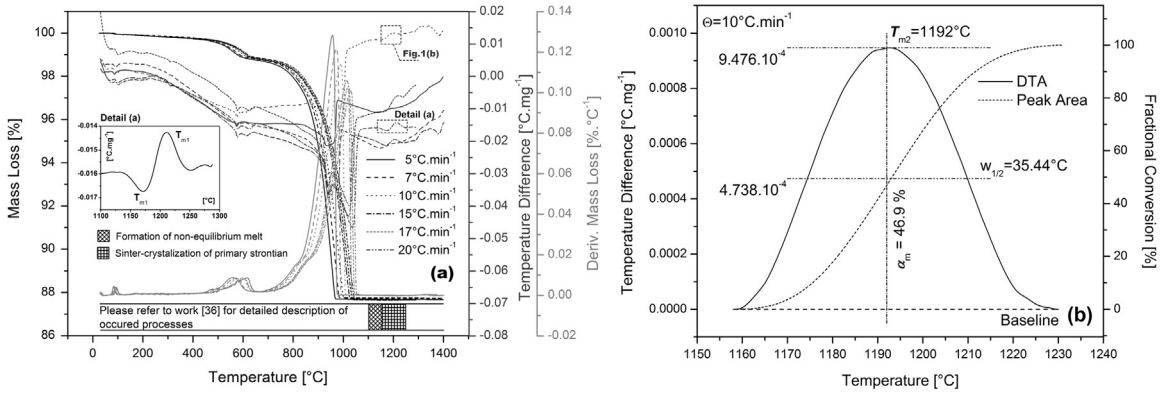

Fig. 1. Thermal analysis or raw meal during the thermal treatment with heating rate from 5 to 20 °C min^{-1} (a) and typical example of evaluation of peak parameters, i.e. $w_{1/2}$ and α_m (b).

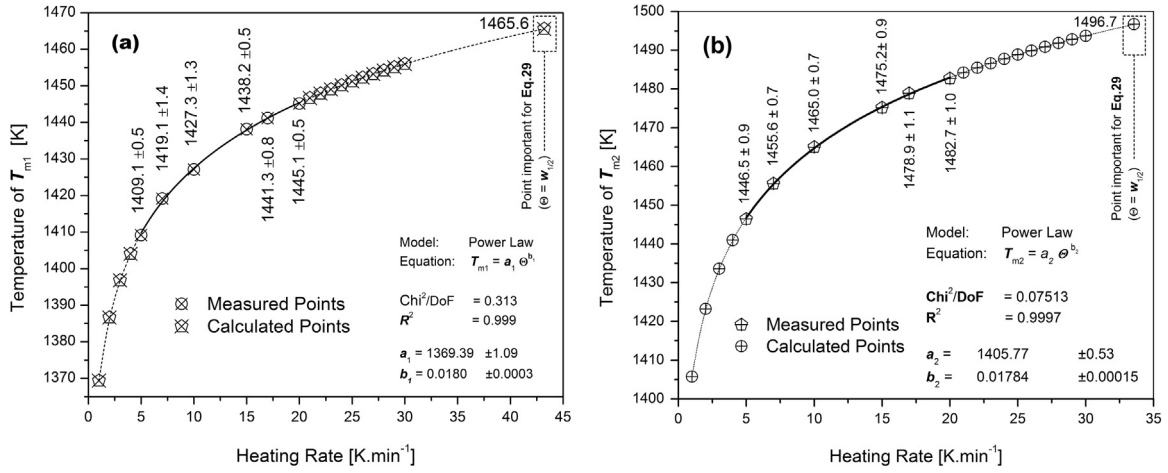

Fig. 2. Influence of heating rate on the temperature of formation of non-equilibrium melt (a) and sinter-crystallization peak of strontian feldspar (b).

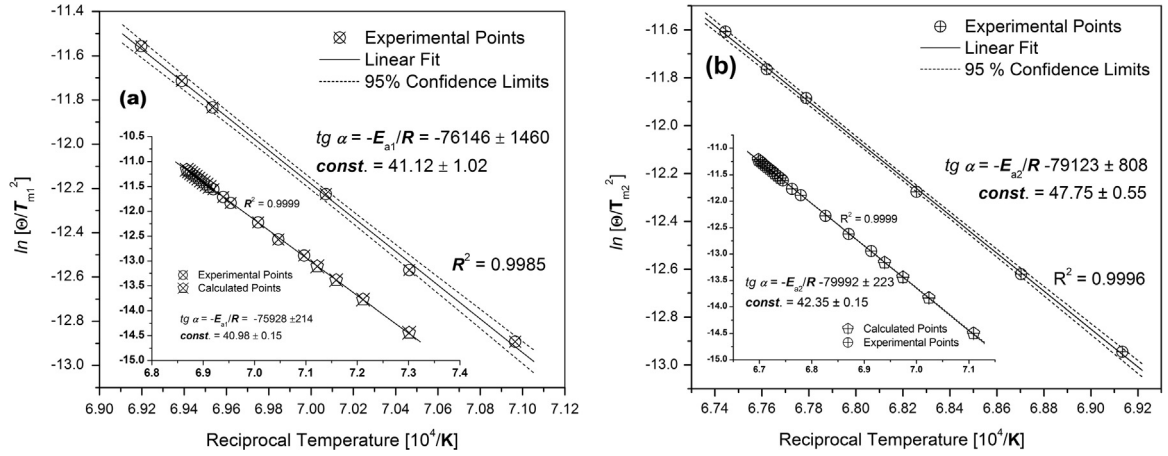

Fig. 3. Kissinger kinetic plot for evaluation of activation energy of formation of non-equilibrium melt (a) and sinter-crystallization of strontian feldspar (b).

Table 1
The overview of kinetic data related to the formation of primary strontian feldspar.

i	Investigated process	Set of data	E_a [kJ mol^{-1}]	A [$\cdot 10^{21}$ s^{-1}]	n for $\Theta \to 1$	$w_{1/2}$ [°C]	α_m [%]
1	Formation of non-equilibrium melt	Experimental	633 ± 24	0.90 ± 2.17	1.4269 ± 0.0026	43.2 ± 3.3	54.3 ± 3.9
		All	631 ± 3	0.71 ± 0.16			
2	Formation of primary strontian feldspar	Experimental	658 ± 7	1.68 ± 0.65	1.8556 ± 0.0036	33.6 ± 2.9	47.4 ± 1.8
		All	664 ± 2	1.66 ± 0.30			

The detail of Fig. 1(a) provides an option to evaluate the process of sinter-crystallization of strontian feldspar (E_{a2}) directly from single DTA experiment. The temperature difference between endothermic peak of formation of non-equilibrium melt (T_{m1}) and exothermic peak of crystallization of primary strontian feldspar (T_{m2}) is independent of the heating rate ($\Delta T_m = T_{m2} - T_{m1} = 37.2 \pm 0.6$ K for Θ from 1 to 30 °C min^{-1}). That means, that the dimensionless value of term $E_{a2}/R(1/T_{m1} - 1/T_{m2})$ must be a constant value (1.40 ± 0.03) as well. The activation energy for the process of sinter-crystallization of strontian feldspar can be then estimated from single DTA measurements as follows:

$$\frac{E_{a2}}{R}\left(\frac{1}{T_{m1}} - \frac{1}{T_{m2}}\right) = const.' = 1.41 \pm 0.02 \quad (17)$$

This behavior results from a specific nature of sinter-crystallization process of non-equilibrium melt. As results from the comparison of Eq. (17) with Eqs. (3) and (37), the left side of this equation is given by the difference $ln\ k_{m2} - ln\ k_{m1} = ln\ (k_{m2}/k_{m1})$. Therefore, the activation energy of both processes must be almost the same ($E_{a1}/E_{a2} = 1.04$). And more importantly, the detail of Fig. 1 (a) also shows, that the temperature of the second inflex point of the peak related to the formation of non-equilibrium melt is the same as the temperature of the first inflex point of the peak of sinter-crystallization of primary strontian feldspar.

In other words, there is no individual temperature region (plateau) related to the non-equilibrium melt. It means, that this in principle thermodynamically unstable melt can be present only in metastable equilibrium with activated state of strontian feldspar and its occurrence must be bond to the reaction zone between original and newly formed phase (it cannot be distributed randomly). The fact, that this behavior requires a certain amount of product at the initial stages of formation of non-equilibrium melt can be explained by the induction period.

The chart of the process mechanism and energetics can be illustrated by Fig. 4(a–c). Since the interlayer of non-equilibrium melt is able to reduce the strain stress on the interface via the change of orientation of newly formed layer of the product (**c**), there is a reason to assume that described mechanism is responsible for mutual polysynthetic or multiple twinning of feldspars (Fig. 4 (c and d)) [36,67]. Since both the processes show mutual highest energetic barrier equal to $\boldsymbol{E}_{a2}$ and $\boldsymbol{E}_{a2}/\boldsymbol{E}_{a1}$ ratio ≈ 1 (Eq. (17)), the sinter-crystallization of strontian feldspar from non-equilibrium melt should be designated as a quazi-isoactivated process.

The analysis of experimental data leads to the deduction and verification of the following approach for single calculation of the activation energy:

$$\sqrt{\frac{E_a}{const.''\ M^{\#}}} = T_{m,\Theta=1} \quad \Rightarrow \quad E_a = const.''\ T^2_{m,\Theta=1} M^{\#} \tag{18}$$

where $\boldsymbol{M}^{\#}$ [kg mol^{-1}] is the molar mass of activated transition-state complex (please refer also to Table 4) the value of which can be estimated for single reactions via the summation $\Sigma(\nu_i \boldsymbol{M}_i)_{products} = \Sigma(\nu_i \boldsymbol{M}_i)_{reactants}$, where ν_i designates the stoichiometric coefficient, or calculated from Eq. (20). Independent variable $\boldsymbol{T}_{m,\Theta=1}$ [K] is the peak temperature (DTA, DTG, DSC, etc.) measured or extrapolated to the heating rate of 1 °C min^{-1}. Hence, the combination of Eqs. (16) and 18 enables to derive more general form of this equation, as follows:

$$E_a\ \Theta^{\frac{2RT_{m,\Theta=1}}{E_a}} = const.''\ T^2_{m,\Theta} M^{\#} \tag{19}$$

That means that the number of required non-isothermal experiments for the determination of activation energy can be reduced to even a single measurement if $\Theta = 1$ °C min^{-1}.

Since the value of term (***const.´´***) is usually close to one, it can be replaced by the average experimental value of 1.12 ± 0.16 (Table 2). This value is in an agreement with the value deduced from Eq. (40) which leads to the term ***const.´´*** = *csch* (***e***) + 1 = 1.1326. Furthermore, ***const.''*** can be also calculated directly for the investigated process using the relation derived from the combination of Eq. (18) with **10** as follows:

$$const.'' = \frac{2.5\ R}{n\ M^{\#} w_{1/2,\Theta=1}} \quad \Rightarrow \quad M^{\#} = \frac{2.5\ R}{const.''\ n\ w_{1/2,\Theta=1}} \tag{20}$$

where the ratio $2\boldsymbol{R}/\boldsymbol{const.''n} = 18.35$ for the reaction of first and pseudo-first order. Eqs. (18) and (19) can be then alternatively used to calculate $\boldsymbol{M}^{\#}$ for the process with known value of activation energy or to eliminate this parameter from Eq. (18):

$$E_a = \frac{2.5\ R}{n\ w_{1/2,\Theta\to 1}}\ T^2_{m,\Theta=1} \tag{21}$$

As can be seen from numerous examples introduced by Table 2, this relation can be used for the investigation of heterogeneous kinetics of wide range of processes with well-defined stoichiometry (Eqs. (18) and (19)) or known reaction order (Eq. (21)), such as the dehydroxylation of clay minerals, the decomposition of carbonates, the synthesis of binary oxides, the preparation of synthetic analogs of minerals, etc.

Although a good agreement can be found between the results calculated by Eq. (18) and the data published in literature (Table 2), there are still questions about the set of parameters leading to the temperature $\boldsymbol{T}_{m,\Theta=1}$ as well as about the nature of constant term. The calculation of $\sqrt{(\boldsymbol{E}_a/\boldsymbol{M}^{\#})}$ term provides the value of 1394.1 and 1421.2 m s^{-1} for the formation of non-equilibrium melt and for sinter-crystallization of strontian feldspar, respectively. Since the rate corresponding to $\sqrt{(\boldsymbol{E}_a/\boldsymbol{M}^{\#})}$ is reached at experimentally measured peak temperature $\boldsymbol{T}_{m,\Theta=1}$, there must be a direct relation between this rate (and value $\boldsymbol{E}_a$ as well) and the peak temperature, which can be solved as follows:

$$\sqrt{\frac{E_a}{const.''\ M^{\#}}} = \sqrt{\frac{RT'}{const.''M^{\#}}} = \sqrt{\frac{\bar{v}_x^2}{const.''}} = T_{m,\Theta=1} \tag{22}$$

where the temperature $\boldsymbol{T}'$ is given by the ratio:

$$\frac{T'}{T_m} = \frac{E_a}{RT_m} \quad \Rightarrow \quad T' = \frac{E_a}{R} = \frac{\bar{v}_x^2}{r} = -\frac{\Delta G^{\#}(T')}{\Delta S^{\#}(T')}\ \left[K\right] \tag{23}$$

That means that:

$$T^2_{m,\Theta=1} = \frac{\bar{v}_x^2}{const.''} = \frac{T'\,r}{const.''} \quad \Rightarrow \quad E_a = \bar{v}_x^2 M^{\#} = \frac{1}{2}\bar{v}^2 M^{\#} = const.''\ T^2_{m,\Theta=1} M^{\#} \tag{24}$$

where the term $\boldsymbol{const.''} = \boldsymbol{RT}'/\boldsymbol{M}^{\#}\boldsymbol{T}_m{}^2 = \boldsymbol{rT}'/\boldsymbol{T}_m{}^2 = \bar{v}_x^2/\boldsymbol{T}_m{}^2$ [m^2 K^{-2} s^{-2}] (please refer to Eq. (18) and Table 2) and $\boldsymbol{r} = \boldsymbol{R}/\boldsymbol{M}^{\#}$ is specific gas constant. The parameter $\bar{v}_x^2 = \bar{v}^2/2$ results from the relation $\bar{v}^2 = (-\bar{v}_x)^2 + \bar{v}_x^2 = 2\bar{v}_x^2$, where the rate along the reaction coordinate is $\bar{v}_x$ and the rate in opposite direction is $-\bar{v}_x$. For the peak of energetic barrier ($\boldsymbol{E}_a$) the parity $-\bar{v}_x = \bar{v}_x$ is supposed. That means that the translation energy $1/2\ M^{\#}\bar{v}^2$(Eq. (24)) of activated state is $\boldsymbol{E}_t = \boldsymbol{E}_a = R\boldsymbol{T}' = \bar{p}^2/\left(2\,M^{\#}\right)$, where the momentum $\bar{p} = M^{\#}\bar{v}$. Therefore, there should be a two translation degree of freedom (***f***), i.e. one degree of freedom for both segments of $\bar{v}$. Therefore, $\boldsymbol{f} = 4$ for the complex of forward and backward reactions.

It is possible to introduce a new term $\boldsymbol{const.'''} = \sqrt{\boldsymbol{const.''}} = \sqrt{(\boldsymbol{rT}')}/\boldsymbol{T}_m$ [m K^{-1} s^{-1}] to Eq. (18), with suggested name "temperature-rate kinetic coefficient", and to write:

$$E_a = \left(const.'''\ T_{m,\Theta=1}\right)^2 M^{\#} \tag{25}$$

As is proved bellow (refer to the discussion to Eqs. (39)–(42)), the value of temperature-rate kinetic coefficient is not a function of α_m and is usually close to one (1.05 ± 0.07). Eq. (18), resp. Eq. (25), is of a general validity, as was proved by the estimation of activation energy for investigated and other numerous examples of heterogeneous processes of different kind (synthesis, crystallization and thermal decomposition of carbonates and clay minerals) which are listed in Table 2. The difference from experimental value is usually very small and does not exceed 0.1%. Since the error for experimental value of ***A*** is usually high (e.g. refer to Table 1), there is also a satisfying confidence between calculated and experimental value of frequency factor.

It could be further derived that:

$$\frac{E_a}{T'} = R; \quad \frac{E_a}{\bar{v}_x^2} = M^{\#}; \quad \frac{E_a}{M^{\#}} = T'\,r = \bar{v}_x^2 = \frac{\bar{v}^2}{2}; \tag{26}$$

and:

$$\frac{T'}{\bar{v}_x^2} = \frac{M^{\#}}{R} = \frac{1}{r}; \quad \frac{T'}{\bar{v}^2} = \frac{M^{\#}}{2R} = \frac{1}{2r}. \tag{27}$$

The value of constant term ***const.´´*** (Eq. (20)) or $(\boldsymbol{const.'''})^2$ can be then used to calculate the frequency factor of investigated process as follows:

$$\begin{aligned} &(a)\quad A = \frac{k_B}{h}\ \exp\left(\frac{n\ w_{1/2,\Theta=1}}{2.5}\right) = \frac{k_B}{h}\ \exp\left(\frac{r}{const.''}\right)\ \left[\Delta S^{\#} > 0\right];\\ &(b)\quad A = \frac{k_B}{h}/\exp\left(\frac{const.''}{r}\right) \approx \frac{k_B}{h}\ \left[\Delta S^{\#} < 0\right]. \end{aligned} \tag{28}$$

That means that expression of Eq. (28) depends on the *sign* ($\Delta \boldsymbol{S}^{\#}$) and $\boldsymbol{r} = \boldsymbol{const.''} \cdot ln\,(\boldsymbol{h}A/\boldsymbol{k}_B)$ for $\Delta \boldsymbol{S}^{\#} > 0$ (**a**) and $\boldsymbol{r} = \boldsymbol{const.''}/ln\,(\boldsymbol{k}_B/\boldsymbol{h}A)$ for $\Delta \boldsymbol{S}^{\#} < 0$ (**b**). It could be also derived from this Eq.

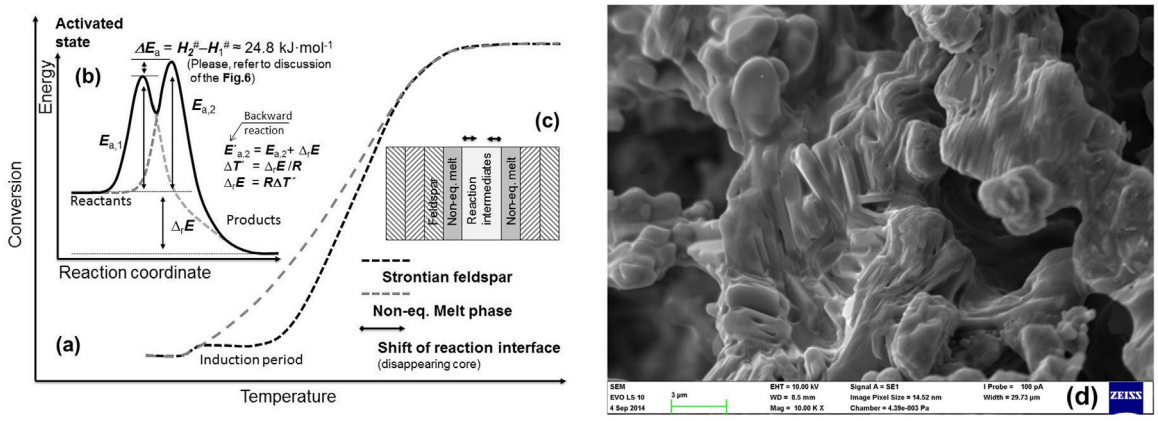

Fig. 4. Simplified scheme which introduces the role of non-equilibrium melt (a), energetics (b) and mechanism (c) of the process of formation of strontian feldspar. SEM image of polysynthetic twins of strontian feldspar treated to the temperature of 1300 °C (d, please refer to [36]).

Table 2
Examples comprising activation energy calculated from Eq. (25) with data published in literature.

i	Investigated process	Calculated kinetic parameters			Published data	
		E_a[kJ mol^{-1}] A [s^{-1}][a]	$T_{m,\Theta=1}$[K]	const.‴ [m K^{-1}s^{-1}]	E_a[kJ mol^{-1}] A [s^{-1}]	Reference
1	Formation of non-equilibrium melt[b]	632 (624; 1.3%) $1.11 \cdot 10^{21}$	1370	1.017	631 and 633[c] $8.98 \cdot 10^{20}$	This article
2	Sinter-crystallization of primary strontian feldspar[b]	658 (658; < 0.1%) $1.46 \cdot 10^{21}$	1406	1.011	658 and 664[c] $1.68 \cdot 10^{21}$	This article
3	Thermal decomposition of α-$SrCO_3$ (rhombohedral)	255 (256; < 0.1%) $2.04 \cdot 10^{10}$	1170	1.125	255[c] $1.58 \cdot 10^{8}$	[68]
4	Thermal decomposition of β-$SrCO_3$ (hexagonal)	231 (226; < 0.1%) $2.04 \cdot 10^{10}$	1161	1.089	227[c] $8.39 \cdot 10^{6}$	
5	Thermal decomposition of $CaCO_3$[f]	189 (189; < 0.1%) $2.06 \cdot 10^{10}$	882	1.064	189[d] $1.23 \cdot 10^{8}$	[69]
6	Dehydroxylation step during treatment of kaolinite	195 (196, < 0.1%)	715	1.214	195[d]	[70,71]
7		176 (176, < 0.1%)	726	1.137	176[d]	[72]
8	Synthesis of SrA	218 (217, < 0.1%)	1131	0.876	218[c]	[73]
9	Dehydroxylation of talc (untreated)	402 (402, < 0.1%) $3.31 \cdot 10^{19}$	1123	0.917	402[d] $3.21 \cdot 10^{15}$	[74]
10	Dehydroxylation of talc (reactive during synthesis)[f]	365 (366, < 0.1%) $5.34 \cdot 10^{18}$	1110	0.883	365[d] $8.29 \cdot 10^{13}$	[69]
11	Formation of spinel phase from calcined kaolin	856 (856; < 0.1%)	1221	1.161	856[c]	[75]
12		954 (954; < 0.1%) –	1187	1.328	954[e] $\Theta \leq 3$ °C min^{-1}	[76]
13		562 (562; < 0.1%) –	1178	1.027	562[e] $\Theta \geq 3$ °C min^{-1}	
14	Dehydroxylation of halloysite (Fabrani Potok, Serbia)	169 (169[g]; 0.1%) –	764	1.019	169[c] –	[77]

[a] Determined with the value of constant term calculated according to Eq. (25), where **const.‴** = $\sqrt{}$**const.″**. The value of E_a results from the term **csch** (**e**)+1=1.1326 (please refer to the discussion to Eqs. (44) and (46)) and $M^{\#}$ from Eq. (20) and its difference from experimental value is introduced in brackets. The value of **A** is given for the cases for which the required data are available.
[b] Calculated with experimental points only (Table 1). As was mentioned above, both processes lead to the same product.
[c] Determined by DTA via the Kissinger kinetic approach.
[d] Determined by DTG via the Kissinger kinetic approach.
[e] Determined by TDA via the Kissinger kinetic approach.
[f] Reactive decomposition which leads to the formation of $Ca_2Al_2O_5$ phase.
[g] The value of $w_{1/2}$ used for the calculation of $M^{\#}$ via Eq. (20) was estimated from Fig. 4 of article [77].

(28) that the value of $A \approx k_B/h$ if $\Delta S^{\#} < 0$ and $(1+e)/(re) < csch\,(r)$ (please refer to discussion of Eq. (43)).

The value of kinetic factor was calculated according to Eq. (10) using assessed value (Fig. 1 (b)) of average peak half-width, which was determined to be 43.2 ± 3.3 and 33.6 ± 2.9 °C for the process of formation of non-equilibrium melt and for sinter-crystallization of strontian feldspar, respectively. The temperature dependence of kinetic factor on the heating rate is shown in Fig. 5. This trend can be accurately described by the power law:

$$n_i = p_i\ \Theta^{s_i} = n_{i,\Theta=1}\ \Theta^{E_{ai}/RT^2_{mi,\Theta=w1/2}} \qquad (29)$$

or via its logarithmic form: $ln\ n_i = s_i ln\ \Theta + ln\ _{pi}$. The parameter $_{pi}$ is given by n for $\Theta = 1$ K min^{-1} and the scaling exponent s_i is equal to the ratio $E_{ai}/RT_{mi,\Theta=w1/2}{}^2 = T'/T_{mi,\Theta=w1/2}{}^2$ $(= RT + \Delta H^{\#}/RT^2 = dln\ k/dT$ [78]), i.e. to the slope of the plot of $ln\,(n_{i,\Theta}/n_{i,\Theta=1})$ on $ln\ \Theta$. That means that the kinetic factor is proportional to the heating rate raised to the s_i power. The value of T_{mi} (calculated from Eq. (16)) for $\Theta = w_{1/2}$ (Fig. 2 and Table 1) is 1465.4 and 1496.0 K for the formation of non-equilibrium melt and for the crystallization of primary strontian, respectively.

The fitted values of parameter p_1 (Fig. 5(a)), i.e. the value of n_1 for $\Theta \to 1$, and s_1 for the process of formation of non-equilibrium

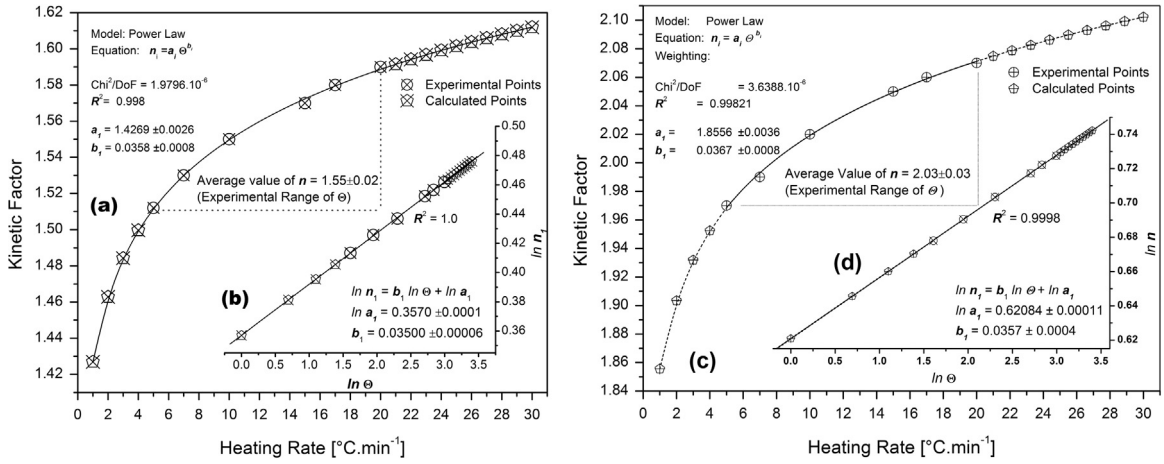

Fig. 5. Influence of heating rate on the value of kinetic factor for the process of formation of non-equilibrium melt (a) and primary strontian feldspar (c). Linearization via logarithmic graph is shown in details (b) and (d).

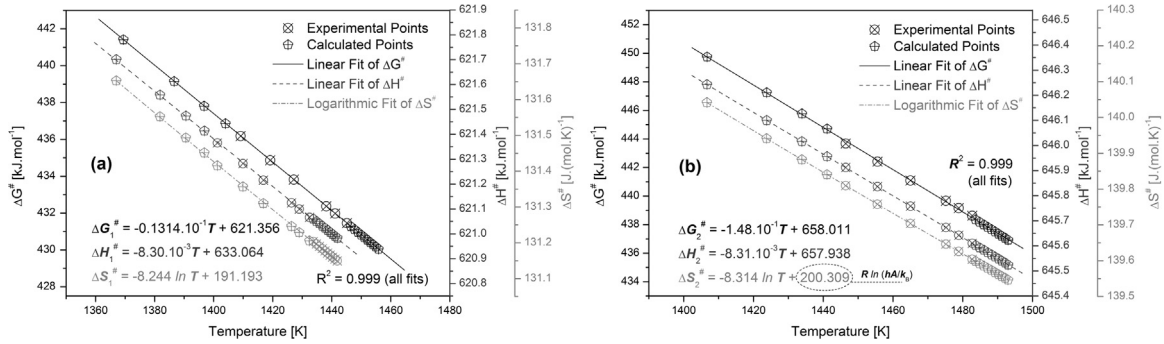

Fig. 6. Temperature dependence of $\Delta G^{\#}$, $\Delta H^{\#}$ and $\Delta S^{\#}$ for activated state: formation of non-equilibrium melt (a) and strontian feldspar (b). Although the temperature dependence of $\Delta S^{\#}$ on this limited experimental temperature range seems linear, the requirement to use the logarithmic function implies from Eq. (12).

melt ($R^2 = 0.998$) are 1.4269 ± 0.0026 and 0.0358 ± 0.0008, respectively. The average value of kinetic factor, which was determined over the experimental range of heating rate, is 1.56 ± 0.02. The values of parameters $p_2 = 1.8556 \pm 0.0036$ and $s_2 = 0.0367 \pm 0.0008$ determined ($R^2 = 1.000$) for the formation of primary strontian from experimental as well as the sum of experimental and calculated results indicate the reaction process of the non-integer order (**b**). The average value of reaction order calculated over the experimental range of Θ is 2.03 ± 0.03.

That enables to determine the mechanism of sinter-crystallization of primary strontian feldspar as the process driven by decreasing nucleation rate of new phase and by the diffusion controlled growth of nuclei [59]. The shape of DTA peak as well as the value resulting from Eq. (17) with the work of Marotta et al. [79] indicate that the nuclei of primary strontian are formed by the surface nucleation. Decreasing amount of non-equilibrium melt with increasing temperature reduces then the nucleation rate while the diffusion growth is accelerated.

The average fractional conversion of the process of formation of non-equilibrium melt (α_{m1}) and primary strontian feldspar (α_{m2}) was determined via the integration of DTA peak to be $54.3 \pm 3.9\%$ and $47.4 \pm 1.8\%$, respectively. The assessed values of n_i and α_{mi} then enable to calculate the frequency factor from the constant term of Kissinger equation (Eq. (9)). The value of frequency factor for the formation of non-equilibrium melt calculated from experimental and from the sum of experimental and extrapolated results is $(0.90 \pm 2.17) \cdot 10^{21}$ and $(7.11 \pm 1.54) \cdot 10^{21}\ s^{-1}$, respectively. The formation of primary strontian feldspar shows the experimental value of $A = (1.68 \pm 0.65) \cdot 10^{21}\ s^{-1}$. For the sum of experimental and extrapolated results the value of $A = (1.66 \pm 0.30) \cdot 10^{21}\ s^{-1}$ (Table 1).

Since the value of $A = \bar{v}_x/\delta = \sqrt{E_a/M^{\#}}/\delta$, the length of energetic barrier (δ) as well as time which is required to overcome this barrier ($t_\delta = \delta/\bar{v}_x$) can be determined to $1.55 \cdot 10^{-18}$ m and $1.11 \cdot 10^{-21}$ s (formation of non-equilibrium melt) and $8.59 \cdot 10^{-19}$ m and $6.02 \cdot 10^{-22}$ s (sinter-crystallization of strontian feldspar). That also means that formation of non-equilibrium melt is the rate-limiting step of this process.

Determined temperature dependences of transition state thermodynamic functions including enthalpy ($\Delta H^{\#}$), entropy ($\Delta S^{\#}$) and Gibbs free energy ($\Delta G^{\#}$) are shown in Fig. 6 for both investigated processes. These results enable to calculate the values of $\Delta H^{\#}$, $\Delta S^{\#}$ and $\Delta G^{\#}$ for standard reference conditions including the temperature of 298.15 K and atmospheric pressure (101325 Pa) and these data are listed in Table 3. Positive value of entropy ($\Delta S^{\#} > 0$) of both processes corresponds to higher probability of formation of activated complex, i.e. the reaction is faster, than in the case when $\Delta S^{\#} < 0$ [80].

The average values of $\Delta H^{\#}$ and $\Delta S^{\#}$ which are determined within investigated interval of heating rate correspond to the parameters of Eyring plot (Fig. 7(a)) and these results are also listed in Table 3. The temperature dependence of $\Delta G^{\#}$ (Fig. 6) enables to calculate the theoretical equilibrium temperature ($\Delta G_1^{\#} = \Delta G_2^{\#}$, where subscripts 1 and 2 correspond to non-equilibrium melt and strontian feldspar) to be 2208 K. Hence, as results from Eq. (13), the term $\Delta H_2^{\#} - \Delta H_1^{\#} = \Delta E_a = 24.9$ kJ mol^{-1} (Fig. 4), and the corresponding difference in $\Delta S_2^{\#} - \Delta S_1^{\#}$ is equal to 11.2 J mol^{-1} K^{-1}.

It is obvious that, the value of $\Delta H^{\#} = 0$ and $\Delta G^{\#} = -T\Delta S^{\#}$ when $T = T' = E_a/R$. Since the dimension of term E_a/R [J mol^{-1}/J K^{-1} mol^{-1} = K] is equal to the temperature (Eq. (23)), the isobaric

Table 3
Thermodynamic parameters of transition-state and the value of rate constant at 298.15 K.

Investigated process of formation of		Data for	$\Delta H^{\#}$ [kJ mol^{-1}]	$\Delta S^{\#}$ [J (K mol)$^{-1}$]	$\Delta G^{\#}$ [kJ mol^{-1}]	k_0 [s^{-1}]
1	non-equilibrium melt phase	298.15 K 101325 Pa	630.6	144.2	582.2	$5.90 \cdot 10^{-91}$
2	primary strontian feldspar		655.5	152.9	613.9	$3.79 \cdot 10^{-95}$
1	non-equilibrium melt phase	Average ($1 \leq \Theta \leq 30$)	621.2	131.3	433.1	–
2	primary strontian feldspar		645.7	148.1	427.9	–
1	non-equilibrium melt phase	Eyring plot (Fig. 7)	621.4	131.4	432.9[a]	–
2	primary strontian feldspar		645.8	148.2	428.0[a]	–

[a] Average value from data calculated for T_{mi} over investigated interval of Θ.

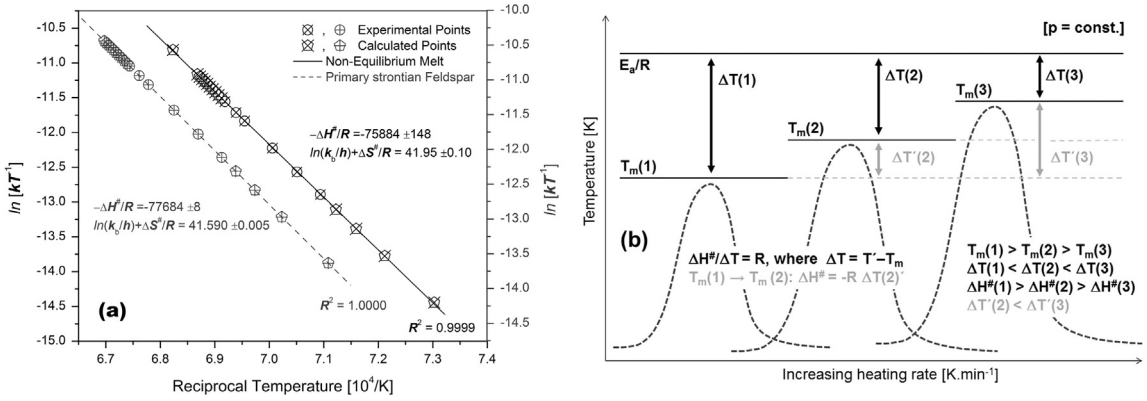

Fig. 7. Eyring plot (a) and schematic drawing of heating rate influence on the enthalpy of activated state (b).

thermal capacity of activated state can be calculated as follows:

$$\frac{\Delta H^{\#}}{\frac{E_a}{R} - T_m} = \frac{\Delta H^{\#}}{\Delta T} = 8.316 \pm 0.004 = R \quad [p] \tag{30}$$

for all values of T_m determined from DTA. The value corresponding to R, can also be derived by the substitution from Eqs. (13)–(30). From that, the temperature dependence of change of enthalpy and entropy of activated state can also be derived (please refer to discussion of Eq. (24)), as follows:

$$\Delta H^{\#}(T_2) = \Delta H^{\#}(T_1) - R \int_{T_2}^{T_1} dT = \Delta H^{\#}(T_1) - R\,(T_2 - T_1) = \Delta H^{\#}(T_1) - p\ \Delta V_m^{\#}; \tag{31}$$

$$\Delta S^{\#}(T_2) = \Delta S^{\#}(T_1) - R \int_{T_2}^{T_1} \frac{dT}{T} = \Delta S^{\#}(T_1) - R\ \ln\frac{T_2}{T_1} = \Delta S^{\#}(T_1) - 2R\ \ln\frac{T_2}{T_1} + R\ \ln\frac{V_{m2}^{\#}}{V_{m1}^{\#}}. \tag{32}$$

That means that the value of $\Delta H^{\#}$ decreases at about isobaric heat $-R\Delta T$ (Eq. (31)), i.e. for reversible isobaric work $-p\Delta V_m^{\#}$, which could be utilized for isobaric expansion [p] during the change of temperature from T_1 to T_2 (Fig. 7(b)), i.e. for the dilatation contribution to the heat capacity of ideal gas. Therefore, it could be further derived (Mayer´s law [81,82]) that the isochoric heat capacity of activated state decreases for the value of $2R$ (Eq. (32)).

The temperature dependences of $\Delta V_m^{\#} = R\Delta T/p$ and $V_m^{\#} = RT/p$ for activated state of primary strontian feldspar are given by the relations $\Delta V_m^{\#} = 8 \cdot 10^{-5} T - 0.0245$ and $V_m^{\#} = 8 \cdot 10^{-5} T - 6 \cdot 10^{-17}$ [m^3 mol^{-1}], respectively. Using the isobaric volume thermal expansion coefficient ($\alpha_{exp.}$) in the expression $\alpha_{exp.} = 1/298.15 = 3.354 \cdot 10^{-3}$ K^{-1}, i.e. for standard reference temperature of 25 °C, it is possible (for any investigated process) to write:

$$V_m^{\#}(T) = V_m^{\#}(298.15) \cdot (1 + 3.354 \cdot 10^{-3} \Delta T); \tag{33}$$

where $V_m^{\#}(298.15\ \mathrm{K}) = 2.446 \cdot 10^{-2}$ m^3 mol^{-1}. The density of activated state can be then calculated as follows:

$$\rho^{\#}(T) = \frac{M^{\#}}{V_m^{\#}(T)} = \frac{p}{rT} = \frac{2.5\ p}{n\ const.''\ w_{1/2,\Theta=1}\ T} = \frac{E_a}{\bar{v}_x^2\ V_m^{\#}(T)}. \tag{34}$$

Since the temperature dependence of $\rho^{\#}$ can be fitted ($R^2 = 1$) by the power law $\rho^{\#} = 3970 T^{-1}$ (hyperbola), where the value of parameter 3970 is given by the ratio $M^{\#}p/R = p/r$, there is an inverse proportionality of $\rho^{\#}$ to temperature. That means that activated-state represents the lowest possible volume density of energy under given pressure ($E_a = RT = pV_m^{\#}(T') \rightarrow p = E_a/V_m^{\#}(T') = const.'' \cdot T_m^2/\rho^{\#}(T')$). The combination of Eqs. (24) and (34) then enables to derive, that:

$$p = \frac{E_a}{V_m^{\#}(T')} = \bar{j}^{\#}(T')\bar{v}_x = \rho^{\#}(T')\bar{v}_x^2 = \frac{1}{2}\rho^{\#}(T')\bar{v}^2; \tag{35}$$

where the mass flux for activated state is $\bar{j}^{\#}(T) = E_a/V_m^{\#}(T)\bar{v}_x$ [kg s^{-1} m^{-2}], i.e. $\bar{j}^{\#}(T') = p/\bar{v}_x$. This behavior also enable to deduce that energetic density of activated state, i.e. kinetics of the process, could be also affected via potential of force field (ϕ), so that it can be written:

$$\frac{1}{2}\rho^{\#}(T')\bar{v}^2 + \rho^{\#}(T')\phi - p = 0. \tag{36}$$

Eq. (11) enables to calculate the value of set of isothermal rate constants, which were presented in the form of Arrhenius plot, i.e. via the dependence of $\ln k$ on the reciprocal temperature, in Fig. 8 (a). The slope ($-E_a/R$) and the intercept ($\ln A$) lead to the same value of activation energy and frequency factor as was previously determined via the Kissinger equation (Eq. (9)). The value of rate constant for the temperature of 25 °C (Table 3), which was determined via the linear fit of Arrhenius plot, can be then used to recalculate to any temperature via the following equation [78]:

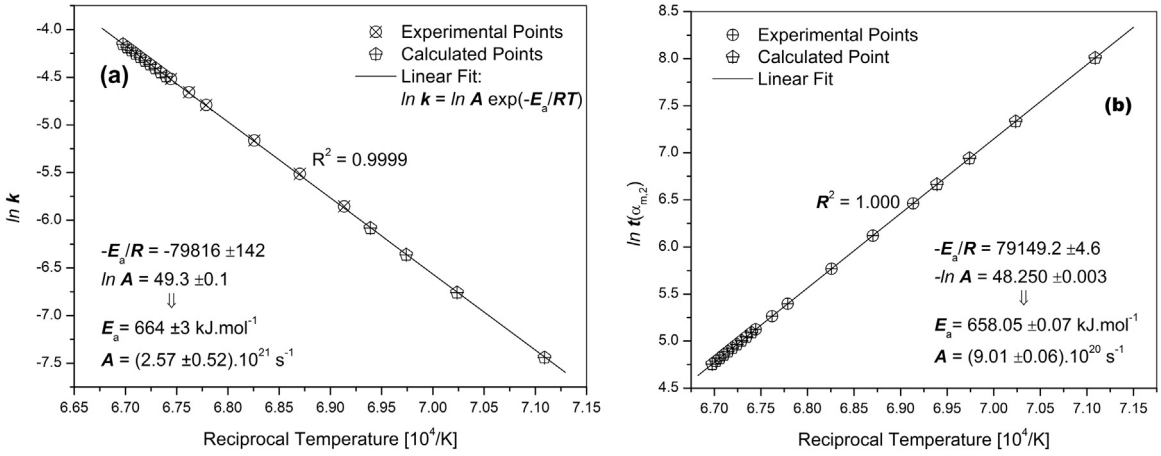

Fig. 8. Arrhenius plot for the process of formation of primary strontian feldspar (a) and the kinetic plot $ln\ \boldsymbol{t}(\alpha_m)$ on $\boldsymbol{T}^{-1}$ (b).

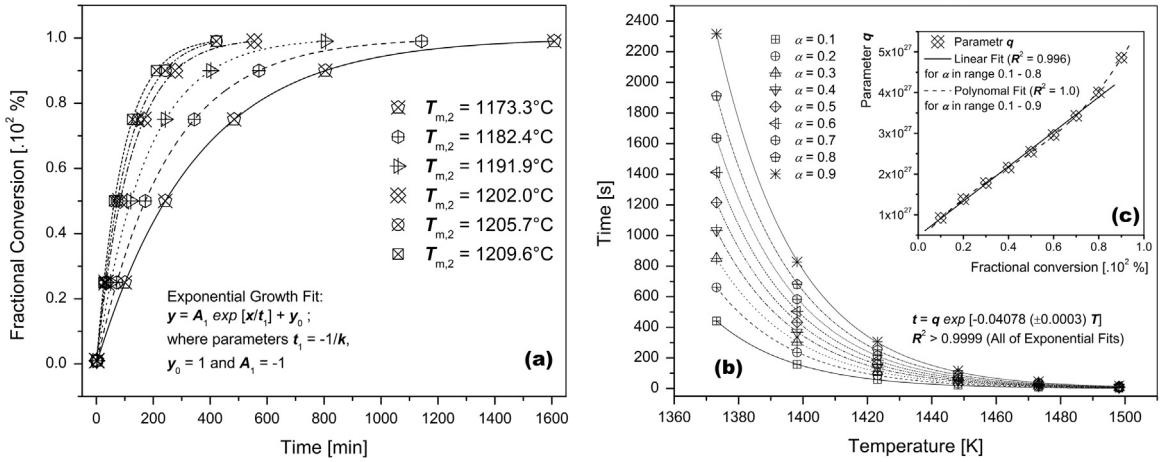

Fig. 9. Formation of primary strontian feldspar under isothermal condition (a) and time required to reach given fractional conversion (b) with depicted dependence of parameter $\boldsymbol{q}$ on α in detail (c).

$$k(T) = k_0 \exp\left[\frac{E_a}{R}\left(\frac{1}{298.15} - \frac{1}{T}\right)\right]. \tag{37}$$

It was empirically found that wide range of mineral reactions can be described by the general form of Eq. (39)·[83]. Further separation of variables and their integration leads to the KJMA equation [59,83], where the term $1/\boldsymbol{n}$ has been incorporated into the rate constant [83]:

$$\frac{d\,\alpha}{d\,t} = k^n t^{n-1}(1-\alpha) \Rightarrow \ldots \Rightarrow \quad \alpha = 1 - \exp\left(-kt\right)^n. \tag{38}$$

Eqs. (37) and (38) can be then used to calculate $\boldsymbol{t}(\alpha_{m2})$, i.e. the time at which the fractional conversion reaches given value of α_{m2} at isothermal temperature corresponding to $\boldsymbol{T}_{m2}$. The value of α_{m2} from Table 1 is used in order to approximate the fixed stage of reaction, i.e. the time at which a fixed transformed fraction of total amount is achieved, by the time when the process reaches the maximum transformation rate. These data also result in the straight line kinetic plot for the dependence of $ln\ \boldsymbol{t}(\alpha_m)$ on reciprocal temperature (Fig. 8(b)), which provides very similar activation energy and frequency factor as Kissinger (Fig. 3(b)) and Arrhenius plot (Fig. 8(a)).

Determined kinetic data were used to estimate the course of the process of formation of primary strontian feldspar under isothermal conditions. The exponential time dependence of fractional conversion for temperatures corresponding to $\boldsymbol{T}_{m2}$ is shown in Fig. 9(a). The temperature dependence of time, which is required to reach given degree of conversion is depicted in Fig. 9(b). These data reveal that the time corresponding to given value of degree of conversion and the temperature can be calculated according to the equations:

$$t_{\alpha m2} = q\ \exp\left(-0.04078\ T\right) \quad [\alpha_{m2}, T]. \tag{39}$$

The value of parameter $\boldsymbol{q}$ can be derived from the linear fit (Fig. 9(c)):

$$q = 4.229{\cdot}10^{27}\ \alpha_{m2} + 4.829{\cdot}10^{26} \quad (0.1 \le \alpha_{m2} \le 0.8); \tag{40}$$

or from the polynomial fit (also depicted in detail (**c**)) as follows:

$$q = 3.125{\cdot}10^{26} + 6.730{\cdot}10^{27}\ \alpha_{m2} - 7.976{\cdot}10^{27}\ \alpha_{m2}^2 + 6.759 \cdot 10^{27}\ \alpha_{m2}^3 \quad (0.1 \le \alpha_{m2} \le 0.9) \tag{41}$$

That means that the parameter ($\boldsymbol{z}$ [K s^2 m^{-2}]) in the term $exp\ (-0.04078\boldsymbol{T}) = exp\ (-\boldsymbol{zT})$ is not a function of α_m (in contrast to parameter $\boldsymbol{q}$). Since the meaning of parameter $\boldsymbol{z}$ could be solved as $1/((\boldsymbol{R}/\boldsymbol{M}^{\#})-1) = \boldsymbol{M}^{\#}/(\boldsymbol{R}-\boldsymbol{M}^{\#}) = 1/(\boldsymbol{r}-1)$, there is a relation to temperature-rate kinetic coefficient (Eq. (25)), which can be expressed by the formula:

$$z = 1/\frac{(const'')^2 T_{m.\Theta=1}^2}{T'} - 1 = 1/\frac{\bar{v}_x^2}{T'} - 1 = \frac{T'}{\bar{v}_x^2 - T'} \tag{42}$$

The combination with (Eqs. (18)–(28)**(a)**) then leads to the expression:

$$E_a = M^{\#}T' \frac{1+z}{z} \quad \Rightarrow \quad \frac{E_a}{M^{\#}T'} = \frac{R}{M^{\#}} = r = const.'' \ln\left(\frac{hA}{k_B}\right) = \frac{1+z}{z}; \tag{43}$$

which explains the relation of parameter $\boldsymbol{z}$ to specific gas constant (Table 4), i.e. $\boldsymbol{r}=(1/\boldsymbol{z})+1 \approx csch\ (\boldsymbol{z})+1$. This relation becomes very accurate if $\boldsymbol{z} < \boldsymbol{e} \approx 2.718$, i.e. when $\boldsymbol{r}=(1+\boldsymbol{z})/\boldsymbol{z} > 1.37$ and $csch\ (\boldsymbol{z})+1 > \boldsymbol{const.}$''. The validity of this law is provided by other experimental evidence for suggested method of estimation of activation energy.

Since the activation energy depends on the hyperbolic function of parameter $\boldsymbol{z}$ (Eq. (43)), it could be written:

$$E_a = M^{\#}T'(\mathrm{csch}(z) + 1) \tag{44}$$

where $csch\ (\boldsymbol{z})=2/(\boldsymbol{e}^{\boldsymbol{z}}-\boldsymbol{e}^{-\boldsymbol{z}})=\boldsymbol{r}-1$ (for $\boldsymbol{z} > 0$) and is the hyperbolic cosecant function. Therefore, $\boldsymbol{z} = arcsch(\boldsymbol{r}-1)=ln\ [(1+\sqrt{(\boldsymbol{z}^2+1)})/|\boldsymbol{z}|]$. For the value of $\boldsymbol{z}=exp\ (\boldsymbol{E}_a/\boldsymbol{RT}')=\boldsymbol{e}$, the value of term $csch\ (\boldsymbol{e})+1=\boldsymbol{const.}''=1.1326$ $(=\boldsymbol{T}'(csch\ (\boldsymbol{z})+1)/\boldsymbol{T}_{m,\Theta=1}{}^2)$ and this value is in excellent agreement with experimental results presented in Table 2.

The substitution of this term to Eq. (18) enables to calculate a plane (Fig. 10(a)), which represents a graphical solution for the dependence of $\boldsymbol{E}_a$ on $\boldsymbol{T}_m$ and $\boldsymbol{M}^{\#}$. The grid of the plane is formed via series of parabolas (with constant mass of activated state $[\boldsymbol{M}^{\#}]$) and straight lines (isotherms $[\boldsymbol{T}_m]$), where the parabola parameters $(\boldsymbol{E}_a=\boldsymbol{P}\cdot\boldsymbol{T}_m{}^2)$ are given by increasing slope of isothermal lines $(\boldsymbol{P}=\boldsymbol{const.}''\boldsymbol{T}_m{}^2)$. These isothermal lines also represent the processes with constant value of $\bar{v}_x^2=\boldsymbol{E}_a/\boldsymbol{M}^{\#}$ (Eq. (26)). Furthermore, the curves parallel to $\boldsymbol{T}_m{}^2-\boldsymbol{M}^{\#}$ plane represent an isoactivated processes $[\boldsymbol{E}_a]$, where:

$$\frac{T_{m1}}{T_{m2}} = \frac{\bar{v}_{x1}}{\bar{v}_{x2}} = \sqrt{\frac{M_2^{\#}}{M_1^{\#}}} \quad \Rightarrow \quad M_2^{\#} = \frac{M_1^{\#}T_{m1}^2}{T_{m2}^2} = \frac{M_1^{\#}\bar{v}_{x1}^2}{\bar{v}_{x2}^2}. \tag{45}$$

Since the temperature (and the translation rate along the reaction coordinate as well (Eq. (24))) of two isoactivated processes is inversely proportional to the square root of the mass of activated state, the expression Eq. (45) is analogical to the Graham´s law of effusion [84]. The combination of Eqs. (13)–(15) and (28) (for $\Delta\boldsymbol{S}^{\#} > 0$, refer to Table 3) enables to calculate a plane for the dependence of $\Delta\boldsymbol{G}^{\#}$ on $\boldsymbol{T}_m$ and $\boldsymbol{M}^{\#}$ (**Fig.10(b)**). The solution for the processes with $\Delta\boldsymbol{S}^{\#} < 0$ and $(\boldsymbol{1}+\boldsymbol{e})/(\boldsymbol{re}) < csch\ (\boldsymbol{r})$ (refer to the discussion of Eq. (28)) is shown in detail (**c**).

Moreover, the hyperbolic cosecant of parameter $\boldsymbol{z}$ can be expanded by the partial fractions as follows [85]:

$$\mathrm{csch}\ (z) = \frac{1}{z} - \frac{2z}{\pi^2+z} + \frac{2z}{4\pi^2+z} - \frac{2z}{9\pi^2+z} + \ldots = \sum_{j=0}^{\infty} (-)^j \frac{z}{j^2\pi^2+z^2}; \tag{46}$$

which naturally leads to almost the same value of $\boldsymbol{const.}''=csch\ (\boldsymbol{e})+1=1.1336$ $(\boldsymbol{j}=30)$ for $\boldsymbol{z}=\boldsymbol{e}$. More importantly, the value of $\boldsymbol{const.}''' = \sqrt{\boldsymbol{const.}''} = 1.0642$ provides the option for the approximation of parameter $\boldsymbol{B}(\boldsymbol{x})$ in empirical equation for Arrhenius temperature integral $\boldsymbol{p}(\boldsymbol{x})$ proposed by **Doyle** [86]:

$$p(x) = 7.03\cdot10^{-3}\ \exp\left[x\ B(x)\right]; \tag{47}$$

via Eq. (47) as follows:

$$B(x) \approx const.''' = \sqrt{\mathrm{csch}\ (e) + 1} = \left[1 + \sum_{j=0}^{\infty} (-)^j \frac{e}{j^2\pi^2+e^2}\right]^{1/2}; \tag{48}$$

which leads to the relation:

$$F(\alpha) \approx \ 7.03\cdot10^{-3} \frac{AE_a}{\Theta R}\ \exp\left[-\frac{1.0642\ E_a}{RT}\right]; \tag{49}$$

where the overview of kinetic function $\boldsymbol{F}(\alpha)=\boldsymbol{kt}$ can be found in the following literature [87–89]. Published value for term $\boldsymbol{B}(\boldsymbol{x})$ ranges from 1.195 to 1.034 with the average value of 1.052 [90,91].

Table 4
Selected function values of $csch\ (z)+1$ for $z > 0$, i.e. for the first quadrant.

z	$csch\ (z)+1$	z	$csch\ (z)+1$	z	$csch\ (z)+1$
($\boldsymbol{e}$) 2.718	(**const.**'')1.1326	0.075	14.321	0.023	44.474
1.000	1.851	0.050	20.992	0.020	50.997
0.750	2.216	[a]0.041	25.513	0.018	56.553
0.500	2.915	0.035	29.556	0.017	59.821
0.250	4.959	0.030	29.556	0.016	63.497
0.100	10.98	0.025	40.996	0.015	67.664

[a] Value corresponding to the sinter-crystallization of strontian feldspar.

4. Conclusion

The investigation of kinetics and thermodynamics of activated state related to the process of sinter-crystallization of primary strontian feldspar from non-equilibrium melt during the thermal treatment of ceramic body reveals a quazi-isoactivated process, where non-equilibrium melt cannot be distributed randomly, but exists only in equilibrium with activated state of strontian feldspar. Since the occurrence of non-equilibrium is restricted to the reaction zone between original and newly formed phase, there is the

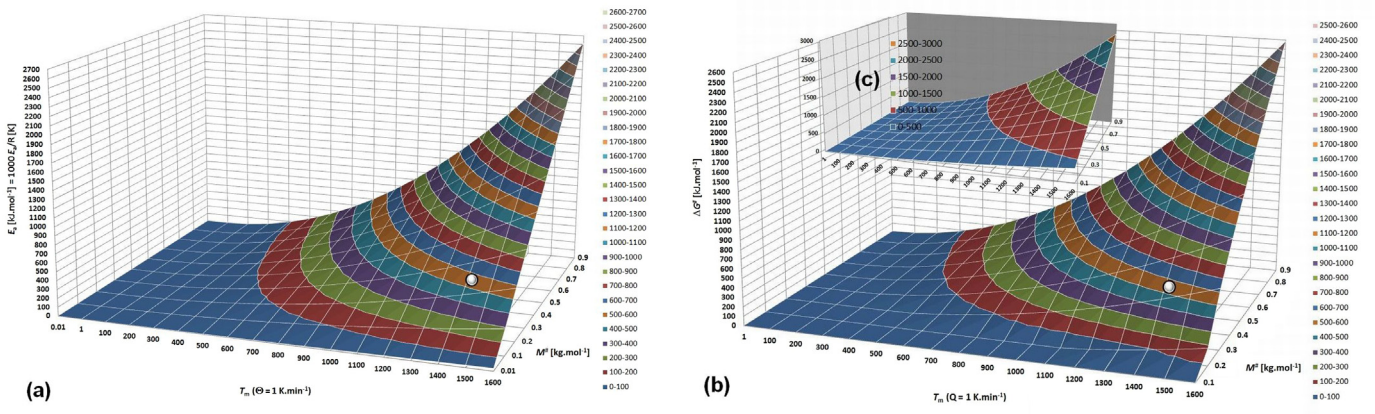

Fig. 10. Dependence of $\boldsymbol{E}_a$ (a) and $\Delta\boldsymbol{G}^{\#}$ (b,c) on $\boldsymbol{T}_m$ and $\boldsymbol{M}^{\#}$ with marked (○) location of the process of formation of primary strontian feldspar.

mechanism, which enables to explain the polysynthetic intergrowth or multiple twining of feldspars.

The process of formation of non-equilibrium melt and subsequent crystallization of primary strontian feldspar requires the activation energy of 631 ± 3 and 664 ± 2 kJ mol^{-1}, respectively. The values of frequency and kinetic factors related to the processes mentioned above are $(7.11 \pm 1.50) \cdot 10^{20}$ and $(1.66 \pm 0.30) \cdot 10^{21}$ s^{-1} and 1.43 a 1.86, respectively. The formation of primary strontian feldspar is then driven by decreasing surface nucleation rate of new phase and diffusion controlled growth of formed nuclei.

Determined kinetic data provide an experimental base to demonstrate new kinetic approach for the determination of activation energy and frequency factor of heterogeneous processes. The investigation of thermodynamics of activated state was used to derive the equation for the temperature dependence of $\Delta H^{\#}$ and $\Delta S^{\#}$. With increasing temperature, e.g. via the shift caused by higher applied heating rate, the value of $\Delta H^{\#}$ and $\Delta S^{\#}$ decreased to about isobaric heat $-R\Delta T$ and $-R \cdot ln\,(T_2/T_1)$, respectively. The density of activated state is inversely proportional to the temperature and the energetic density of activated state is equal to the pressure.

Moreover, the translation rate along the reaction coordinate is inversely proportional to the square root of the mass of activated state. Further investigation of kinetic data reveals that the activation energy is directly proportional to the term $csch\,(z)+1$. For $z=e$, this term enables to derive the value for parameter $B(x)$ in empirical equation for the Arrhenius temperature integral $p(x)$ proposed by Doyle to 1.0642 which is in good agreement with the average value from published experimental data.

Acknowledgments

The paper was supported by the project Materials Research Center at FCH BUT – Sustainability and Development, REG LO1211, with financial support from National Programme for Sustainability I (Ministry of Education, Youth and Sports, Czech Republic).

References

[1] D. Emery, A. Robinson, Inorganic Geochemistry: Applications to Petroleum Geology, Blackwell Scientific Publications, Oxford, United Kingdom, 2009.
[2] L.V. Pirsson, Petrography and geology of the igneous rocks of the Highwood mountains, Montana, Bulletin 237 (1905).
[3] J.S. Diller, H.B. Patton, The geology and petrography of Crater Lake National Park, Ser. Geol. Surv. Prof. Pap. 105–107 (1902).
[4] J. Gerrard, Fundamentals of Soils, Taylor & Francis Group, London, New York, 2000.
[5] G. Sposito, The Chemistry of Soils, Oxford University Press, New York, 2008.
[6] E. El-Meliegy, R. van Noort, Glasses and Glass Ceramics for Medical Applications, Springer New York, New York, 2012.
[7] C.B. Carter, M.G. Norton, Ceramic Materials: Science and Engineering, Springer-Verlag, New York, 2007.
[8] F. Singer, Industrial Ceramics, Springer, Dordrecht, Netherlands, 2013.
[9] A.O. Surendranathan, An Introduction to Ceramics and Refractories, CRC Press, Taylor & Francis Group, Boca Raton, London, New York, 2014.
[10] E.S. Bastin, Geology of the Pegmatites and Associated Rocks of Maine: Including Feldspar, Quartz, Mica and Gem Deposits, U.S. Government Printing Office, Washington, DC, 1911.
[11] M. De Graef, M.E. McHenry, Structure of Materials: An Introduction to Crystallography, Diffraction and Symmetry, Cambridge University Press, Cambridge, 2007.
[12] J.V. Smith, Feldspar Minerals: 2 Chemical and Textural Properties, Springer Science & Business Media Springer, Berlin Heidelberg, Berlin, 1974.
[13] M.M. Krzmanc, B. Jančar, D. Suvorov, The influence of tetrahedral ordering on the microwave dielectric properties of Sr0.05Ba0.95Al2Si2O8 and (M=Al, Ga, M′=Si, Ge) ceramics, J. Eur. Ceram. Soc. 28 (16) (2008) 3141–3148.
[14] E. Wiberg, N. Wiberg, Inorganic Chemistry, Academic Press, London, 2001.
[15] J.R. Goldsmith, Gallium and germanium substitutions in synthetic feldspars, J. Geol. 58 (5) (1950) 518–536.
[16] Y.-M. Sung, S. Kim, Sintering and crystallization of off-stoichiometric $SrO \cdot Al_2O_3 \cdot 2SiO_2$ glasses, J. Mater. Sci. 35 (17) (2000) 4293–4299.
[17] Y.-P. Fu, C.-C. Chang, C.-H. Lin, T.-S. Chin, Solid-state synthesis of ceramics in the BaO–SrO–Al_2O_3–SiO_2 system, Ceram. Int. 30 (1) (2004) 41–45.
[18] C. Ferone, B. Liguori, A. Marocco, S. Anaclerio, M. Pansini, C. Colella, Monoclinic (Ba, Sr)-celsian by thermal treatment of (Ba, Sr)-exchanged zeolite A, Microporous Mesoporous Mater. 134 (1–3) (2010) 65–71.
[19] Y. Kobayashi, M. Inagaki, Preparation of reactive Sr-celsian powders by solid-state reaction and their sintering, J. Eur. Ceram. Soc. 24 (2) (2004) 399–404.
[20] A. Marocco, B. Liguori, G. Dell'Agli, M. Pansini, Sintering behaviour of celsian based ceramics obtained from the thermal conversion of (Ba, Sr)-exchanged zeolite A, J. Eur. Ceram. Soc. 31 (11) (2011) 1965–1973.
[21] N.P. Bansal, J.A. Setlock, Fabrication of fiber-reinforced celsian matrix composites, Composites Part A 32 (8) (2001) 1021–1029.
[22] W. Lei, R. Ang, X.-C. Wang, W.-Z. Lu, Phase evolution and near-zero shrinkage in $BaAl_2Si_2O_8$ low-permittivity microwave dielectric ceramics, Mater. Res. Bull. 50 (2014) 235–239.
[23] N. Fréty, A. Taylor, M.H. Lewis, Microstructure and crystallisation behaviour of sol-gel derived 1/2SrO-1/2BaO-Al_2O_3-$2SiO_2$ glass-ceramic, J. Non-Cryst. Solids 195 (1–2) (1996) 28–37.
[24] M.F.M. Zawrah, N.M. Khalil, Preparation and characterization of barium containing refractory materials, Ceram. Int. 27 (3) (2001) 309–314.
[25] L. Barbeeri, A.B. Corradi, C. Leonelli, T. Manfredini, M. Romagnoli, C. Siligardi, The microstructure and mechanical properties of sintered celsian and strontium-celsian glass-ceramics, Mater. Res. Bull. 30 (1) (1995) 27–41.
[26] M. Chen, W.E. Lee, P.F. James, Synthesis of monoclinic celsian glass-ceramic from alkoxides, J. Non-Cryst. Solids 147–148 (1992) 532–536.
[27] A.S. Radosavljević-Mihajlović, M.D. Prekajski, J. Zagorac, A.M. Došen, S. S. Nenadović, B.Z. Matović, Preparation, structural and microstructural properties of $Ba_{0.64}Ca_{0.32}Al_2Si_2O_8$ ceramics phase, Ceram. Int. 38 (3) (2012) 2347–2354.
[28] L.A. Orlova, N.V. Popovich, N.E. Uvarova, A. Paleari, P.D. Sarkisov, High-temperature resistant glass-ceramics based on Sr-anorthite and tialite phases, Ceram. Int. 38 (8) (2012) 6629–6634.
[29] F. Clabau, A. Garcia, P. Bonville, D. Gonbeau, T. Le Mercier, P. Deniard, S. Jobic, Fluorescence and phosphorescence properties of the low temperature forms of the $MAl_2Si_2O_8$:Eu^{2+} (M=Ca, Sr, Ba) compounds, J. Solid State Chem. 181 (6) (2008) 1456–1461.
[30] S. Ye, Z.-S. Liu, X.-T. Wang, J.-G. Wang, L.-X. Wang, X.-P. Jing, Emission properties of Eu^{2+}, Mn^{2+} in $MAl_2Si_2O_8$ (M=Sr, Ba), J. Lumin. 129 (1) (2009) 50–54.
[31] X. Zheng, Q. Fei, Z. Mao, Y. Liu, Y. Cai, Q. Lu, H. Tian, D. Wang, Incorporation of Si-N inducing white light of $SrAl_2Si_2O_8$:Eu2+,Mn2+ phosphor for white light emitting diodes, J. Rare Earths 29 (6) (2011) 522–526.
[32] X. Yu, X. Xu, T. Jiang, H. Yu, P. Yang, Q. Jiao, J. Qiu, Tunable color emitting of $CaAl_2Si_2O_8$: Eu, Tb phosphors for light emitting diodes based on energy transfer, Mater. Chem. Phys. 139 (1) (2013) 314–318.
[33] X. Yu, X. Xu, P. Yang, Z. Yang, Z. Song, D. Zhou, Z. Yin, Q. Jiao, J. Qiu, Photoluminescence properties and the self-reduction process of $CaAl_2Si_2O_8$:Eu phosphor, Mater. Res. Bull, 47, (2012) 117–120.
[34] M. Ma, D. Zhu, C. Zhao, T. Han, S. Cao, M. Tu, Effect of Sr2+-doping on structure and luminescence properties of BaAl2Si2O8: Eu2+ phosphors, Opt. Commun., 285, (2012) 665–668.
[35] V.B. Pawade, N.S. Dhoble, S.J. Dhoble, Rare earth (Eu^{2+},Ce^{3+}) activated $BaAl_2Si_2O_8$ blue emitting phosphor, J. Rare Earths 32 (7) (2014) 593–597.
[36] P. Ptacek, F. Soukal, T. Opravil, E. Bartonickova, J. Wasserbauer, The formation of feldspar strontian ($SrAl_2Si_2O_8$) via ceramic route: reaction mechanism, kinetics and thermodynamics of the process, Ceram. Int. 42 (7) (2016) 8170–8178.
[37] W. Pannhorst, J. LÖHn, Zur Kristallstruktur von Strontianit, $SrCO_3$, Z. Krist. – Cryst. Mater. 131 (1970) 455.
[38] M.J. Starink, The determination of activation energy from linear heating rate experiments: a comparison of the accuracy of isoconversion methods, Thermochim. Acta 404 (1–2) (2003) 163–176.
[39] H.E. Kissinger, Reaction kinetics in differential thermal analysis, Anal. Chem. 29 (11) (1957) 1702–1706.
[40] R.L. Blaine, H.E. Kissinger, Homer Kissinger and the Kissinger equation, Thermochim. Acta 540 (0) (2012) 1–6.
[41] J. Farjas, P. Roura, Exact analytical solution for the Kissinger equation: determination of the peak temperature and general properties of thermally activated transformations, Thermochim. Acta 598 (2014) 51–58.
[42] J. Šesták, Thermo-Physical Properties of Solids – Their Measurements and Theoretical Thermal Analysis: Part D, Elsevier Science Publishers, Amsterdam, New York, 1984.
[43] M.E. Brown, D. Dollimore, A.K. Galwey, Reactions in the Solid State Comprehensive Chemical Kinetics, Elsevier, Amsterdam, 1980.
[44] J.E. House, Principles of Chemical Kinetics, Elsevier Science, United States of America, 2007.
[45] S. Vyazovkin, Isoconversional Kinetics of Thermally Stimulated Processes, Springer International Publishing, Switzerland, 2015.
[46] C.M. Guldberg, P. Waage, Studier over Affiniteten [Studies of Affinity], Norwegian Academy of Sciences, Norway 1864, pp. 35–45.
[47] C.M. Guldberg, P. Waage, Studier over affiniteten [The study of affinity], in: Otto Bastiansen (Ed.), The Law of Mass Action – A Centenary Volume, Universitetsforlaget, Diet Norske Videnskaps-Akademi, 1864, pp. 7–17.
[48] C.M. Guldberg, P. Waage, Ueber die chemische affinitate [About chemical affinity], J. Prakt. Chem. 19 (69–114) (1879).
[49] S. Arrhenius, P. pamphlets, Über dIE Dissociationswärme und den Einfluss der Temperatur auf den Dissociationsgrad der Elektrolyte, Wilhelm Engelmann,

Leipzig, 1997.
[50] D. Chen, X. Gao, D. Dollimore, A generalized form of the Kissinger equation, Thermochim. Acta 215 (1993) 109–117.
[51] J. Llópiz, M.M. Romero, A. Jerez, Y. Laureiro, Generalization of the kissinger equation for several kinetic models, Thermochim. Acta 256 (2) (1995) 205–211.
[52] F. Agresti, An extended Kissinger equation for near equilibrium solid–gas heterogeneous transformations, Thermochim. Acta 566 (2013) 214–217.
[53] E.S. Freeman, B. Carroll, The Application of thermoanalytical techniques to reaction kinetics: the thermogravimetric evaluation of the kinetics of the decomposition of calcium oxalate monohydrate, J. Phys. Chem. 62 (4) (1958) 394–397.
[54] P. Budrugeac, E. Segal, Applicability of the Kissinger equation in thermal analysis, J. Therm. Anal. Calorim. 88 (3) (2007) 703–707.
[55] M.E. Brown, P.K. Gallagher, Handbook of thermal analysis and calorimetry. in: Handbook of Thermal Analysis and Calorimetry, 5, Elsevier Science B.V., Amsterdam, The Netherlands, 2008 (pp. ii).
[56] P. Roura, J. Farjas, Analytical solution for the Kissinger equation, J. Mater. Res. 24 (10) (2009) 3095–3098.
[57] J.A. Augis, J.E. Bennett, Calculation of the Avrami parameters for heterogeneous solid state reactions using a modification of the Kissinger method, J. Therm. Anal. 13 (2) (1978) 283–292.
[58] C.S. Ray, Q. Yang, W.-h Huang, D.E. Day, Surface and internal crystallization in glasses as determined by differential thermal analysis, J. Am. Ceram. Soc. 79 (12) (1996) 3155–3160.
[59] J. Málek, The applicability of Johnson-Mehl-Avrami model in the thermal analysis of the crystallization kinetics of glasses, Thermochim. Acta 267 (0) (1995) 61–73.
[60] V. Marghussian, Nano-Glass Ceramics: Processing, Properties and Applications, Elsevier Science, Amsterdam, The Netherlands, 2015.
[61] D.W. Urry, Henry Eyring (1901–1981): a 20th century physical chemist and his models, Math. Model. 3 (6) (1982) 503–522.
[62] M.C. Gupta, Statistical Thermodynamics, New Age International (P) Limited, New Delhi, 2007.
[63] K.A. Connors, Chemical Kinetics: The Study of Reaction Rates in Solution, University of Wisconsin, Madison, 1990.
[64] T.S.L. Radhika, T.K.V. Iyengar, T.R. Rani, Approximate Analytical Methods for Solving Ordinary Differential Equations, CRC Press, Boca Raton, London, New York, 2014.
[65] M.R. Wright, Fundamental Chemical Kinetics: An Explanatory Introduction to the Concepts, Woodhead Publishing, 1999.
[66] A.S. Wightman, N. Balazs, W. Kohn, Part I: Physical Chemistry. Part II: Solid State Physics, Springer, Berlin Heidelberg, 2013.
[67] P. Ptáček, T. Opravil, F. Šoukal, J. Havlica, R. Holešinský, Kinetics and mechanism of formation of gehlenite, Al–Si spinel and anorthite from the mixture of kaolinite and calcite, Solid State Sci. 26 (2013) 53–58.
[68] P. Ptáček, E. Bartoníčková, J. Švec, T. Opravil, F. Šoukal, F. Frajkorová, The kinetics and mechanism of thermal decomposition of SrCO3 polymorphs, Ceram. Int. 41 (1 Part A) (2015) 115–126.
[69] P. Ptacek, K. Lang, F. Soukal, T. Opravil, E. Bartonickova, L. Tvrdik, Preparation and properties of enstatite ceramic foam from talc, J. Eur. Ceram. Soc. 34 (2) (2014) 515–522.
[70] P. Ptacek, F. Frajkorova, F. Soukal, T. Opravil, Kinetics and mechanism of three stages of thermal transformation of kaolinite to metakaolinite, Powder Technol. 264 (2014) 439–445.
[71] P. Ptacek, F. Soukal, T. Opravil, J. Havlica, J. Brandstetr, The kinetic analysis of the thermal decomposition of kaolinite by DTG technique, Powder Technol. 208 (1) (2011) 20–25.
[72] A. Teklay, C. Yin, L. Rosendahl, M. Bøjer, Calcination of kaolinite clay particles for cement production: a modeling study, Cem. Concr. Res. 61–62 (2014) 11–19.
[73] P. Ptacek, F. Soukal, T. Opravil, E. Bartonickova, M. Zmrzly, R. Novotny, Synthesis, hydration and thermal stability of hydrates in strontium-aluminate cement, Ceram. Int. 40 (7) (2014) 9971–9979.
[74] P. Ptacek, T. Opravil, F. Soukal, J. Havlica, J. Masilko, J. Wasserbauer, Preparation of dehydroxylated and delaminated talc: meta-talc, Ceram. Int. 39 (8) (2013) 9055–9061.
[75] P. Ptacek, F. Soukal, T. Opravil, M. Noskova, J. Havlica, J. Brandstetr, The kinetics of Al-Si spinel phase crystallization from calcined kaolin, J. Solid State Chem. 183 (11) (2010) 2565–2569.
[76] P. Ptacek, F. Soukal, T. Opravil, J. Havlica, J. Brandstetr, Crystallization of spinel phase from metakaoline: the nonisothermal thermodilatometric CRH study, Powder Technol. 243 (2013) 40–45.
[77] D. Prodanović, Ž.B. Živković, S. Radosavljević, Kinetics of the dehydroxylation and mullitization processes of the halloysite from the Farbani Potok locality, Serbia, Appl. Clay Sci. 12 (3) (1997) 267–274.
[78] R.K. Bansal, Organic Reaction Mechanisms, Tata McGraw-Hill Education, New Delhi, 1998.
[79] A. Marotta, A. Buri, F. Branda, Nucleation in glass and differential thermal analysis, J. Mater. Sci. 16 (1981) 341–344.
[80] J.W. Moore, R.G. Pearson, Kinetics and Mechanism, Wiley, New York, 1961.
[81] S.C. Garg, R.M. Bansal, C.K. Ghosh, Thermal Physics, Tata McGraw-Hill Education, New Delhi, 2013.
[82] B.M. Askerov, S. Figarova, Thermodynamics, Gibbs Method and Statistical Physics of Electron Gases, Springer, Berlin Heidelberg, 2009.
[83] A. Putnis, An Introduction to Mineral Sciences, Cambridge University Press, Cambridge, 1992.
[84] J.C. Kotz, P.M. Treichel, J. Townsend, D. Treichel, Chemistry & Chemical Reactivity, Cengage Learning, United States, 2014.
[85] K.B. Oldham, J. Myland, J. Spanier, An Atlas of Functions: With Equator, the Atlas Function Calculator, Springer, New York, 2010.
[86] C.D. Doyle, Estimating isothermal life from thermogravimetric data, J. Appl. Polym. Sci. 6 (24) (1962) 639–642.
[87] W.W. Wendlant, Thermal Methods of Analysis, John Wiley Sons, New York, 1974.
[88] J.-d Nam, J.C. Seferis, A composite methodology for multistage degradation of polymers, J. Polym. Sci. Part B: Polym. Phys. 29 (5) (1991) 601–608.
[89] M. Day, J.D. Cooney, D.M. Wiles, A kinetic study of the thermal decomposition of poly(aryl-ether-ether-ketone) (PEEK) in nitrogen, Polym. Eng. Sci. 29 (1) (1989) 19–22.
[90] R.E. Lyon, An integral method of nonisothermal kinetic analysis, Thermochim. Acta 297 (1) (1997) 117–124.
[91] S. Mallakpour, M. Taghavi, The accuracy of approximation equations in the study of thermal decomposition behaviour of some synthesized optically active polyamides, Iran. Polym. J. 18 (2009) 857–872.